CORE
Metadata, citation and similar papers at core.ac.uk
Provided by AIR Universita degli studi di Milano

In situ attenuated total reflection infrared spectroscopy study of the photocatalytic steam reforming of methanol on Pt/TiO_2.

Gian Luca Chiarello[a,*], Davide Ferri[b], Elena Selli[a]

[a]*Dipartimento di Chimica, Università degli Studi di Milano, Via Golgi 19, I-20133 Milano, Italy*

[b]*Paul Scherrer Institut, CH-5232 Villigen, Switzerland*

ABSTRACT

The effect of Pt particle size deposited on TiO_2 on the photocatalytic steam reforming of methanol was studied by *in-situ* attenuated total reflectance infrared spectroscopy (ATR-IR). Two 0.5 wt.% Pt/TiO_2 samples were investigated, one possessing Pt nanoparticles of *ca.* 5 nm size and the other Pt clusters below 2 nm size showing significant different photoactivity both in terms of hydrogen production rate and selectivity to CO, CO_2 and all other by-products. The presence of Pt nanoparticles strongly affects both the adsorption/desorption and the reactivity properties of the TiO_2 surface and reduces the extent of photopromoted conduction band and shallow trapped electrons (*i.e.* increased electron-hole separation). Reducing the Pt size from nanoparticles to clusters increases the rate of methanol and water absorption and hinders the detrimental formation of irreversibly adsorbed CO on Pt. All of these aspects contribute to increase the photocatalytic performance of Pt cluster-decorated TiO_2 with respect to Pt nanoparticles containing TiO_2. Finally, prolonged exposure of all samples to methanol/water vapour in the dark lead to the formation of unreactive formate which persist also under UV-vis irradiation. By contrast, these spectator species do not form when the sample is exposed to methanol/water vapour under UV-vis irradiation.

***Keywords*:** Photocatalytic hydrogen production, *in situ* ATR-IR, Flame Spray Pyrolysis (FSP), Pt clusters

.

* Corresponding author. Tel: +39 02 503 14281; fax: +39 02 503 14300.
E-mail address: gianluca.chiarello@unimi.it

1. Introduction

Photocatalytic reactions became very attractive in the last years for their applications in green chemistry both in the fields of water and air detoxification, and for solar to chemical energy conversion and storage (*i.e.* as hydrogen or hydrocarbons solar fuels). The latter processes occur under anaerobic conditions, with water acting as the oxidant, and are characterised by a positive standard Gibbs free energy change (up-hill reactions). The photocatalyst is a semiconductor able to absorb light because of the electron transition from the valence (VB) to the conduction (CB) band. The so formed electron-hole pairs promote redox reactions on the photocatalyst surface. The major problem, responsible for the usual low quantum efficiency of photocatalytic reactions, is the high probability of charge carriers recombination before promoting any surface reaction. In the case of photocatalytic hydrogen production the efficiency can be effectively enhanced by modifying the semiconductor surface with noble metal nanoparticles, *e.g.* Pt and Au, (able to capture CB electrons) and by adding more efficient hole scavengers in the reaction mixture such as methanol [1].

The photocatalytic steam reforming of methanol, occurring in gas phase, proceeds according to the following reaction:

$$CH_3OH + H_2O \rightarrow CO_2 + 3\ H_2 \qquad (1)$$

In a previous work, we deeply investigated the mechanism of this reaction and found that methanol is oxidized to formaldehyde, formic acid, and finally to CO_2 through both a direct and an indirect mechanism depending on the methanol-to-water ratio [2]. In the direct mechanism, prevailing at high ratio, methanol reacts directly with the VB holes. In the indirect mechanism, prevailing at low ratio, methanol reacts with hydroxyl radicals produced by the reaction of water with VB holes. Carbon monoxide, methane, methyl formate, acetaldehyde and dimethyl ether were also identified as side products [1]. Moreover, the selectivity to all of these intermediates and by-products strongly depends on several factors, including the TiO_2 crystal structure [3], surface modification with noble

metals [1,4] and TiO_2 doping (*e.g.* with fluoride [5]). In the case of Pt modified TiO_2, the selectivity was also affected by the preparation method, *i.e.* by the Pt particle size and distribution [1]. For example, the selectivity to CO of TiO_2 P25 and of two 0.5 wt% Pt catalysts prepared by deposition of preformed Pt nanoparticles on P25 and in single step by flame spray pyrolysis (possessing smaller Pt particle size) was 17.7%, 8.3% and 1.1%, respectively [1]. The hydrogen production rate (and selectivity to CO_2) of these samples was 0.36 (10.7%), 7.75 (17.5%) and 14.23 $mmol_{H_2}$ h^{-1} g_{cat}^{-1} (21.6%), respectively.

Infrared spectroscopy has been widely used to study the interactions of methanol and water with the TiO_2 surface [6–10] and to provide information on the mechanism of photoreaction [10–15]. In addition to the detection of surface species formed during the photoreaction, time resolved FT-IR spectroscopy proved to be a powerful tool to distinguish between photogenerated electrons in the form of free conduction band (CB) and shallow trapped (ST) electrons and to evaluate their lifetime [8,16–18].

In this work, we investigate the behaviour of TiO_2 and of two Pt/TiO_2 by *in situ* ATR-IR spectroscopy during the photo-steam reforming of methanol in order to get a deeper insight into the origin of their photoactivity difference. The two Pt/TiO_2 were selected because of their different Pt particle size of *ca.* 5 nm (*i.e.* Pt nanoparticles) and below 2 nm (*i.e.* Pt clusters because their size is comparable to the Fermi wavelength of an electron [19]). In particular, we studied: *i*) CO, methanol and water/methanol adsorption in the dark in a pulsed mode to follow the corresponding surface interaction dynamics; *ii*) the effect of UV-vis irradiation on the reactivity of the surface species formed after methanol adsorption in the dark (*i.e.* post-irradiation); and *iii*) the effect of UV-vis pre-irradiation on methanol adsorption and reactivity under irradiation.

2. Experimental

2.1. Photocatalysts preparation and characterisation

The two 0.5 wt% Pt modified TiO_2 samples were prepared by two different methods as already described [1]. FP-Pt/TiO_2 was synthesized in continuous and single step by flame spray pyrolysis (FP) [20] by burning an organic solution prepared by mixing 10 mL of titanium(IV)-isopropoxide with 35 mL of xylene and 5 mL of acetonitrile. The proper amount of platinum acetyl acetonate as the Pt precursor was added to the solution.

RM-Pt/TiO_2 was prepared by deposition of preformed Pt nanoparticles on commercial TiO_2 P25 (Evonik), according to the reverse micelle (RM) method [22]. The colloidal suspension of surfactant-stabilized Pt nanoparticles was obtained by adding $NaBH_4$ ($NaBH_4$:Pt 4:1 molar ratio) to a n-dodecyl-trimethylammonium chloride aqueous solution containing platinum acetyl acetonate (surfactant:Pt 40:1 molar ratio). The P25 powder was ultrasonically dispersed in water and then mixed to the Pt colloidal suspension under vigorous stirring. The precipitated grey powder was separated by centrifugation, thoroughly washed with water, and dried overnight in oven at 70 °C [5]. All chemicals were purchased from Aldrich and used as received.

The two photocatalysts were characterised by N_2 adsorption/desorption at 77 K in a Micromeritics ASAP 2010 apparatus to determine their BET specific surface area. The morphology was investigated by high angular annular dark field–scanning transmission electron microscopy (HAADF-STEM) on a JEOL FS2200-FEG instrument, operated at 200 kV. The crystal structure was determined by X-ray diffraction, by recording the XRD patterns with a Philips PW3020 powder diffractometer using the Cu K-α radiation.

2.2. Infrared spectroscopy investigation

In situ attenuated total reflection infrared (ATR-IR) spectroscopy measurements were performed during CO adsorption and methanol photo-steam reforming using an infrared spectrometer (Vector

22, Bruker Optics) equipped with a liquid-N_2 cooled MCT detector and a homemade ATR cell (Fig. 1). The cell allowed irradiation of UV-vis light through two sapphire windows connected to a deuterium and halogen lamp (DH-2000, Ocean Optics) *via* a bifurcated optical fibre (Ocean Optics). For CO adsorption experiments in the dark, *ca*. 5 mg of the sample were deposited on the ZnSe internal reflection element (IRE, 45°, 50 x 20 x 2 mm) after drying of an aqueous suspension in ambient air. The resulting coating covered an area of 5 cm^2. For the photocatalytic experiments, the catalyst layer (*ca.* 1 mg) was prepared by depositing a 2x100 μl aliquot of an aqueous suspension of the catalyst on two spots (d = 5 mm each) over the IRE using a Teflon mask and was left drying in air overnight. The two spots represent the area irradiated by the bifurcated optical fibre.

CO adsorption from the gas phase was followed while flowing 10 vol% CO/N_2 (30 mL/min) for 30 min, followed by purging with N_2 (30 mL/min) for 20 min. Methanol and methanol/water vapour adsorption experiments were performed by bubbling 30 mL/min of N_2 in a *x* vol% CH_3OH/H_2O solution (*x* = 100, 80, 20 or 1%) at 30°C. Spectra were typically collected at 4 cm^{-1} resolution by co-adding 20 scans while the catalyst coating was kept at 30°C.

The main characteristic absorption bands of all detected species during this infrared investigation are summarised in Table 1.

3. Results and discussion

3.1. Photocatalyst characterisation

One step FP-made Pt/TiO_2 exhibits *ca.* 53% anatase and 47% rutile crystal phase composition and a 70 m^2 g^{-1} BET specific surface area. HAADF-STEM analysis (Fig. 2A) shows that the powder consisted of micro-aggregates of TiO_2 single crystal nanospheres, 10-25 nm in diameter. RM-Pt/TiO_2 maintains the structure typical of commercial P25 TiO_2 consisting of widely irregularly shaped, *ca*. 20 nm in size crystalline aggregates, composed of *ca*. 80% anatase and 20% rutile with a specific surface area of 48 m^2 g^{-1}.

HAADF-STEM is a powerful technique to distinguish nanoparticles of heavy elements, because they appear as bright dots due to their different Z-contrast with respect to the lighter metal oxide support. The comparison of the HAADF-STEM images of the two Pt decorated samples (Fig. 2) reveals a significantly different particle size distribution. The analysis of the FP-made evidences the presence of well-dispersed, *ca*. 1.5-2 nm-sized Pt clusters. By contrast, the sample prepared by deposition of preformed Pt nanoparticles exhibits larger (5-6 nm) and partially aggregated Pt nanoparticles. The FP method confirmed to be an effective method to directly produce well dispersed and ultrafine noble metal nanoparticles deposited on a metal oxide support.

3.2. CO adsorption

The interaction of the hydrated surface of TiO_2 P25 as well as of the two Pt modified samples with flowing 10% CO/N_2 led to the transient formation of an intense band at 1640 cm^{-1} followed by a shoulder at 1586 cm^{-1} within the first 10 min (Fig. 3). These bands are attributed to the ν(C=O) stretching mode of adsorbed formic acid and to the antisymmetric stretching (ν_{AS}(OCO)) of adsorbed formate in the bridging bidentate mode [21–25], respectively. These transient species are the intermediates of the surface oxidation of CO to CO_2 through the reaction with adsorbed water and hydroxyl groups on the titania surface. This reaction proceeded up to the consumption of the active hydroxyl groups, conferring the transient behaviour to these species. Moreover, in the spectra of RM-Pt/TiO_2 a transient band also appears at 1723 cm^{-1} attributed to the ν(C=O) mode of adsorbed formaldehyde [21,25,26].

The ATR-IR spectra of adsorbed CO recorded at 30°C on the two Pt/TiO_2 samples (Fig. 4) exhibit at least four signals in the Pt-CO region (2200-1800 cm^{-1}): *i*) a weak and broad signal at 2180 cm^{-1} attributed to CO adsorbed on Ti^{4+} cations [27]; *ii*) bands at 2070 cm^{-1} and *iii*) 2054 cm^{-1} attributed to adsorbed CO on Pt atoms located at terrace and edge sites, respectively [28,29]; *iv*) a broad and weaker signal at 1820 cm^{-1} due to bridge adsorbed CO on the Pt–Pt and Pt–Ti sites [30]. As shown in Fig. 3, a significantly different CO adsorption kinetics is observed on the two samples: a fast

saturation (within the first 30 s) of the defect sites of RM-Pt/TiO_2 (2054 cm^{-1}) is followed by a slower intensification of the band at 2070 cm^{-1}. Similar behavior was reported by Leibsle, *et al.* [28]. The spectrum recorded after saturation with CO (Fig. 4) shows a single band centred at 2070 cm^{-1}. By contrast, both signals grow simultaneously on the FP-made sample, the signal at 2054 cm^{-1} being always more intense than that at higher wavenumbers, and the intensity remained unperturbed under flowing nitrogen.

A comparison between the spectra recorded on the two Pt-containing samples after saturation with CO and purging with N_2 (Fig. 4) reveals that a greater fraction of Pt-defect sites (edges and corners) is present in the FP-Pt/TiO_2, whereas terrace sites prevailed on the RM-Pt/TiO_2. Moreover, FP-Pt/TiO_2 shows a two-fold more intense band, *i.e.* a higher CO adsorption capability. These results confirm the higher Pt dispersion of the FP sample. The smaller the Pt particles, the higher the surface Pt atoms accompanied by an increase of the edge to terrace atoms ratio. This is consistent with the particle size distribution observed by HAADF-STEM analysis (Fig. 2) and represents a significant difference between Pt nanoparticles in RM-Pt/TiO_2 and Pt clusters in FP-Pt/TiO_2. Reducing the Pt size from nanoparticles to clusters not only increases the number of surface active sites for hydrogen reduction, but also affects their nature in favor of the lower coordinated surface atoms. It is nowadays widely accepted that edges are more efficient active sites for several catalytic applications [31]. The predominance of Pt edge sites in FP-Pt/TiO_2 therefore contributes to explain its significant higher photocatalytic activity in hydrogen production.

Formaldehyde also forms on RM-Pt/TiO_2, as indicated by the band at 1720 cm^{-1}, but not on TiO_2 or on FP-Pt/TiO_2. We can therefore tentatively suppose that it is produced by reduction of CO on the Pt terrace sites.

3.2. Methanol adsorption

The ATR-IR spectra recorded on RM-Pt/TiO_2 and on TiO_2 after consecutive pulses of methanol vapours at 30°C are shown in Fig. 5. While FP-Pt/TiO_2 was saturated already after five pulses,

saturation of RM-Pt/TiO_2 occurred more slowly and was reached only after 15 consecutive pulses, indicating a faster absorption kinetics over the flame made material. Various signals appear upon contact of methanol vapours with the samples. Several authors reported, based on IR spectroscopy experiments [6–10] and theoretical calculations [32–34], that methanol adsorbs on TiO_2 both molecularly (CH_3OH_{ads}) and dissociatively with the formation of surface methoxy groups (CH_3O_{ads}). The former species displays C–H antisymmetric ($\nu_{as,C-H}$) and symmetric ($\nu_{s,C-H}$) stretching modes at 2950 and 2845 cm^{-1} (b and c in Fig.5), respectively, and C–O stretching (ν_{C-O}) at 1048 cm^{-1} (i in Fig. 5). The corresponding signals of the methoxy species are slightly shifted towards lower energy, *i.e.* at 2925, 2821 and 1033 cm^{-1} (b', c' and i' in Fig. 5). The C-H bending (δ_{C-H}) mode is found in the 1480-1340 cm^{-1} region for both species (f in Fig. 5). Moreover, mono and bidentate bonding geometries for the methoxy group on TiO_2 have been reported [7,22,32,35]. The two modes can be distinguished by the position of ν_{C-O} at 1126 cm^{-1} (h in Fig. 5) for the monodentate and at 1033 cm^{-1} in the bidentate species.

The appearance of signals due to adsorbed methanol was accompanied by both the displacement of water (negative signals at 3400 and 1625 cm^{-1}, g in Fig. 5) and by the consumption of surface hydroxyl groups (negative bands at 3691 and 3623 cm^{-1}, a and a' in Fig. 5) [10,18,36–38]. At saturation, the signals of adsorbed methanol on RM-Pt/TiO_2 were slightly less intense than those on TiO_2, as observed also by Chen *et al.* [10], due to partial surface coverage by the noble metal. In contrast, the flame made photocatalyst, possessing a higher surface area, displayed more intense signals and therefore improved methanol adsorption capability (Fig. 6).

A noticeable difference between RM-Pt/TiO_2 and FP-Pt/TiO_2 consists in the broad band centred at 2028 cm^{-1} (d in Fig. 5) in the Pt-CO region, which intensified with increasing number of methanol pulses. This band can be attributed to the formation of CO adsorbed on Pt. The formation of this band was already observed [26] also upon ethanol adsorption [15].

The *in situ* ATR-IR spectra recorded during the first pulse of methanol vapours on the three samples are shown in Fig. 6. The upper curve of each group of spectra corresponds to the transit and

diffusion of methanol vapours into the pores of the catalyst layer. Three transient bands (arrows in Fig. 6) can be distinguished at 1640, 1586 and 1360 cm^{-1} especially in the case of RM-Pt/TiO_2, which are ascribed to the ν(C=O) mode of adsorbed formic acid and to the ν_{AS}(O-C-O) and ν_S(O-C-O) modes of adsorbed formate or methyl formate [21–24], respectively. The faster methanol adsorption over the FP-made material, as observed during the pulsed experiments, can reasonably lead to a higher turnover frequency (TOF), *i.e.* a superior catalytic efficiency compared to RM-Pt/TiO_2 in agreement with the results of our photocatalytic tests [1].

The ATR-IR spectra recorded under flowing methanol vapour (instead of successive pulses) presented in Fig. 7 show that the intensity of the two signals at 1640 and 1586 cm^{-1} slightly decreased within 400 s before steady state conditions were attained, which was accompanied by the parallel increase of the signals at 1033 cm^{-1} of the ν(C-O) mode of methanol and at 1170 cm^{-1} of the ν_{AS}(C-O-C) mode of dimethyl ether [39]. In our previous work, dimethyl ether was found to be a major by-product of the photo-steam reforming of methanol [1]. Based on these observations we can conclude that adsorbed methanol undergoes the following surface reactions in the dark at 30°C:

$$CH_3OH_{(g)} + OH_{ads} \rightarrow CH_3O_{ads} + H_2O_{(g)} \quad (2)$$

$$CH_3OH_{(g)} + \square \rightarrow CH_3OH_{ads} \quad (3)$$

$$CH_3O_{ads} + OH_{ads} \xrightarrow{-H_2} HCO_2H_{(g)} + 2\square \quad (4)$$

$$CH_3O_{ads} + OH_{ads} \xrightarrow{-H_2} HCO_2H_{(ads)} + \square \quad (5)$$

$$2CH_3O_{ads} \xrightarrow{-H_2} HCO_2CH_{3ads} \quad (6)$$

$$CH_3O_{ads} + CH_3OH_{ads} \rightarrow CH_3OCH_{3(g)} + OH_{ads} \quad (7)$$

where □ indicates an adsorption site. Moreover, the oxidative dehydrogenation of methanol to CO occurs on Pt:

$$CH_3O_{ads} \xrightarrow{-H_2} H_2CO_{ads} \xrightarrow{-H_2} CO_{ads} \quad (8)$$

The initial decrease of the signals (within 400 s) is attributed to the consumption of surface hydroxyls (reaction 4). Moreover, at least two different types of reactive surface hydroxyls may be present on the surface: weakly bonded hydroxyls accounting for the formation and desorption of

formic acid (reaction 4) and more strongly bonded ones responsible for the residual adsorbed formic acid and formate. Because the production of molecular hydrogen is expected to occur on Pt, reactions (4)-(6) take place very likely at the Pt–TiO_2 interface. This explains why these surface reactions are not observed with TiO_2.

3.3. Methanol/water co-adsorption

As mentioned above, methanol adsorption is accompanied by the displacement of water, *i.e.* methanol and water adsorb competitively on the same sites. Fig. 8 shows that this phenomenon is reversible. When the methanol saturated TiO_2 surface was exposed to consecutive 1 mL pulses of water vapour, the bands characteristic of adsorbed methanol progressively decreased simultaneously to the increase of those of adsorbed water and hydroxyl groups. Interestingly, the displacement of methanol by water was faster on both Pt-loaded samples. In this case, the negative bands at 3691 and 3623 cm^{-1} and the bands in the C–H stretching region fully disappear already after the first pulse of water vapours. This result is consistent with the faster methanol adsorption/desorption kinetics observed on FP-Pt/TiO_2.

The effects of different methanol to water molar fraction in the pulses, *x*, are presented in Fig. 8. When the catalyst was saturated under flowing methanol/water vapours for 30 min followed by purging with N_2, the intensity of the characteristic bands of adsorbed methanol increased with increasing *x* in the feeding vapour mixture parallel to the decrease (negative bands) of those of water and hydroxyls. Noteworthy, the spectra also show the appearance of intense bands in the C=O stretching region due to the formation of surface adsorbed formate and formic acid. These bands are significantly more intense than those recorded in the presence of methanol vapours due to the larger abundance of surface reactive hydroxyl groups supplied by the presence of water in the gas phase. The intensity of these bands also increased with increasing methanol-to-water partial pressure ratio. Furthermore, compared to TiO_2, both Pt modified samples show the appearance of intense bands at 1458 cm^{-1} and at 1640 cm^{-1} characteristic of dimethyl ether and formic acid, respectively. Thus, the

presence of Pt nanoparticles strongly affects the adsorption/desorption properties and the reactivity of the TiO_2 surface, a result that was predicted by DFT calculations. For example, Han *et al.* [34] reported that Pt clusters enhance both molecular methanol adsorption and methanol dissociation via C-O scission on the anatase surface by introducing new active sites at the Pt–TiO_2 interface characterised by a lower activation energy. Moreover, the energy difference between different bond-breaking modes depends on the size of Pt clusters.

3.3. Effect of UV-vis irradiation

Two types of experiments were performed in order to study the effect that UV-vis irradiation has on methanol adsorption and reactivity: *i*) saturation in the dark in flowing methanol vapours followed by irradiation in N_2 atmosphere; *ii*) saturation under UV-vis irradiation in flowing methanol or methanol/water vapours followed by purging in the dark in flowing N_2. By the first type of test we investigated the photocatalytic reactivity of residual surface adsorbed species after methanol saturation. The second type of test allows following the photocatalytic activity under flowing methanol or methanol/water vapours and, after purging in N_2, to evaluate the effect of UV-vis irradiation on the adsorption properties of the photocatalyst. In both types of experiments, FP-Pt/TiO_2 and RM-Pt/TiO_2 behaved similarly (unless specified). Thus, for simplicity, we will focus the discussion on the comparison between TiO_2 and RM-Pt/TiO_2.

3.3.1 Effect of UV-vis irradiation on pre-adsorbed methanol in the dark

As shown in the previous section, prolonged exposure to methanol vapours in the dark leads to the formation of surface formate along with adsorbed methanol and methoxy groups. These species are stable in the dark under N_2 flow. As the photocatalyst layer was irradiated with UV-vis light an absorption-shift of the spectra was observed (Fig. 10). This absorption shift is attributed to the formation of both photopromoted conduction band (CB) and shallow trapped (ST) electrons [8,16–18]. In particular, CB electrons provoke a distinct exponential absorption growth of the IR baseline

while ST electrons give rise to broad bands due to the optical excitation of electrons from the ST states into the CB. Thus, the exact position of these bands depends on the energy difference between ST and CB and are usually located around 1600 cm^{-1} (*ca.* 0.2 eV below the CB). As shown in Fig. 10, the IR absorbance at 1900 cm^{-1} (*i.e.* where no other species are expected to absorb) in the case of TiO_2 increased to a larger extent than for the Pt-modified catalysts, indicating a lower concentration of CB and ST electrons in the absence of Pt. In the presence of Pt, the majority of photopromoted electrons are transferred to and trapped by the Pt nanoparticles. This confirms the capability of Pt to increase the charge carriers separation, with the consequent enhancement of the photocatalytic efficiency. Fig. 10a shows that, as the UV-vis light was switched on, the intensity of all the characteristic bands of adsorbed methoxy species (2925, 2821, 1425 and 1033 cm^{-1}) decreased. These signals fully disappeared after 80 min irradiation on TiO_2 and after 30 min irradiation on RM-Pt/TiO_2. Comparing the blue curves of Fig. 11, it is evident that no bands of adsorbed formaldehyde (1727 and 1502 cm^{-1}), formic acid (1710 cm^{-1}) or dimethyl ether (2733 and 1710 cm^{-1}) remained in the spectra after UV-vis irradiation, contrarily to the spectra recorded in the dark. Thus, these species either fully desorbed or reacted under irradiation, leading to the gaseous products of the photosteam reforming reaction reported in our previous work [1,2]. In contrast, residual bands of formate (2865, 1586, 1383 and 1360 cm^{-1}), methylformate (2970 cm^{-1}), and adsorbed CO on Pt at 2010 cm^{-1} persisted on the photocatalyst surface, proving the accumulation of oxidative products with a high bonding energy (spectator species). Particularly detrimental is the persistence of CO adsorbed on Pt for its poisoning effect that very likely contributes to the lower photocatalytic activity of RM-Pt/TiO_2 compared to FP-Pt/TiO_2. Some relevant difference between RM-Pt/TiO_2 and TiO_2 arises when comparing the C-H stretching region (Fig. 10a). After exposing TiO_2 to UV-vis light, residual bands of unreacted methoxy groups persisted and the bands of methylformate and formates were significantly weaker, confirming the superior photoactivity of the Pt containing photocatalyst in the complete photo-assisted oxidation of adsorbed methanol.

3.3.2 Methanol and methanol/water adsorption on UV-vis irradiated TiO_2 surface

These experiments were performed under constant UV-vis irradiation of the photocatalyst layer. In particular, the photocatalyst was pre-irradiated for 30 min under N_2 flow, and then the IR background was recorded. Methanol or methanol/water adsorption was first performed (five consecutive pulses) and then the photocatalyst was exposed to a continuous flow of methanol or methanol/water vapours for 30 min, followed by 30 min purging with N_2. Some remarkable differences arise when comparing the same experiments in dark (blue curves of Fig. 11) and under UV-vis irradiation (red curves of Fig. 11), namely:

i) Surface methanol saturation occurred faster on all pre-irradiated samples.

ii) No negative bands appear in the 3750-3550 cm^{-1} region indicating no consumption of surface hydroxyl groups during methanol adsorption, *i.e.* these species were very likely removed during pre-irradiation.

iii) Contrarily to the experiment performed in the dark, in the ATR-spectra recorded *in situ* under flowing methanol and methanol/water vapours, the transient bands of adsorbed formic acid (1640 cm^{-1}) and formates (1586 and 1360 cm^{-1}) completely disappear after purging with N_2. Thus, formates did not accumulate on the TiO_2 surface upon UV-vis irradiation of the photocatalyst, even after prolonged exposure to methanol vapours.

iv) The bands of adsorbed methanol were more stable after purging with N_2 under UV-vis light than those formed in the dark. Thus, these methanol species are slowly photo-oxidised.

v) The band at 2028 cm^{-1} due to CO adsorbed on Pt was weaker when methanol or methanol/water were adsorbed under UV-vis light.

UV-vis pre-irradiation is known to affect the surface properties of TiO_2, *e.g.* by inducing TiO_2 surface hydrophilicity [40]. Photopromoted electrons can be transferred to surface Ti^{4+}, forming Ti^{3+} sites, whereas holes can create oxygen vacancies. These two phenomena very likely consume hydroxyl groups and adsorbed water and increase the surface concentration of free sites for faster methanol adsorption. Moreover, UV-vis irradiation increases the surface reactivity of TiO_2, *i.e.*

methanol is oxidised to formate (as shown in the spectra recorded during methanol vapours exposure), but they do not accumulate on the surface (as occurs by contrast in the dark), because they desorb or are further oxidised up to CO_2. Thus, present results suggest that pre-irradiation of the photocatalysts, prior to the photocatalytic tests, might increase their performance.

4. Conclusions

In situ ATR-IR investigation of methanol photo-steam reforming on Pt/TiO_2 demonstrated that the promoting effect of Pt on photocatalytic performance is not only limited to its ability to enhance the charge carrier separation by trapping the CB electrons. The presence of Pt introduce new active sites at the $Pt–TiO_2$ interface that strongly affect the adsorption/desorption dynamics and reactivity of methanol and water. Pt particle size also plays a crucial role. Pt clusters (*i.e.* with size < 2 nm) on titania, produced in single step by flame spray pyrolysis, proved to be co-catalysts more effective than Pt nanoparticles. Reducing the Pt particle size below 2 nm not only increases the surface to bulk Pt atom ratio, but also the edge and corners to terrace Pt atoms ratio. The lower coordinated Pt atoms located at edges and corners are expected to be more reactive and to prevent the formation of poisoning CO adsorbed on Pt after exposure to methanol vapours.

Finally, the adsorption/desorption dynamics and reactivity are also affected by the UV-vis irradiation that prevents the formation of unreactive formate.

Acknowledgments

Part of this work was performed at the Swiss Federal Laboratories for Materials Science and Technology (Empa, Switzerland). Dr. M.H. Aguirre is acknowledged for recording the HAADF-STEM images.

Tables

Table 1: Main IR absorption bands of the identified species adsorbed on TiO_2

Specie	**Absorption mode**	**Wavenumber / cm^{-1}**	**Ref.**
Molecular methanol (CH_3OH_{ads})	$\nu_{as,C-H}$ $\nu_{s,C-H}$ ν_{C-O} δ_{C-H}	2950 2845 1048 1480-1340	[6–10]
Monodentate methoxy (CH_3O_{ads})	$\nu_{as,C-H}$ $\nu_{s,C-H}$ ν_{C-O} δ_{C-H}	2925 2821 1128 1480-1340	[6–10]
Bidentate methoxy (CH_3O_{ads})	$\nu_{as,C-H}$ $\nu_{s,C-H}$ ν_{C-O} δ_{C-H}	2925 2821 1033 1480-1340	[7,22,32,35]
Physisorbed water (H_2O_{ads})	ν_{H-O-H} δ_{H-O-H}	3400 1625	[10,18,36–38]
Hydroxyl groups (Ti-OH)	$\nu_{as,O-H}$ $\nu_{s,O-H}$	3691 3623	[10,18,36–38]
Formate ($HCOO_{ads}$)	$\nu_{,C-H}$ $\nu_{as,C-O}$ $\nu_{s,C-O}$ δ_{C-H}	2865 1586 1360 1383	[21–25]
Formic acid ($HCOOH_{ads}$)	$\nu_{s,C=O}$	1640	[21–25]
Formaldehyde (H_2CO_{ads})	$\nu_{s,C=O}$ δ_{C-H}	1727 1502	[21,25,26]
Dimethyl ether ($(CH_3)_2O_{ads}$)	$\nu_{as,C-H}$ δ_{C-H} ρ_{C-H} $\nu_{s,C-O-C}$	2979 1458 1170 918	[39]
Ti(IV)-CO		2180	[27]
Pt-CO	Terrace Edge Bridged	2070 2054 1820	[28,29] [30]

Figure captions

Fig. 1: Sketch of the homemade *in situ* ATR-IR cell. The IR beam is reflected towards the ZnSe crystal, while the sample thin film is irradiated on top with UV-vis light through two sapphire windows connected to the bifurcated optical fibres.

Fig. 2: HAADF-STEM images of FP-Pt/TiO_2 (A) and MR-Pt/TiO_2 (B). Pt nanoparticles appear as bright spots on the titania support because of their higher Z-contrast.

Fig. 3: (a) *In situ* ATR-IR spectra and (b) time on stream evolution of selected signals recorded at 30°C during exposure to flowing 10% CO/N_2 for 30 min followed by purging with N_2 for 20 min. Symbols: (♦) 2180 cm^{-1} of TiO_2-CO, (●) 2070 cm^{-1} of Pt-$CO_{terrace}$, (▲) 2054 cm^{-1} of Pt-CO_{edge}, (x) 1720 cm^{-1} of formaldehyde, (Δ) 1640 cm^{-1} of formic acid, and (+) 1586 cm^{-1} of formate. The arrow indicates the beginning of N_2 purging.

Fig. 4: Comparison of *in situ* ATR-IR spectra in the Pt-CO region recorded with the two Pt modified TiO_2 samples after saturation in flowing 10% CO/N_2 for 30 min followed by purging with N_2 for 20 min.

Fig. 5: Comparison of *in situ* ATR-IR spectra recorded at 30°C on hydrated bare and Pt modified TiO_2 after 1, 2, 3, 10 (grey lines) and 15 (black bold line) consecutive pulses of 1 mL N_2 saturated with methanol vapours at 30°C, followed by N_2 purging for 10 min. Peaks attribution is reported in Table 1 and in the text.

Fig. 6: Evolution of *in situ* ATR-IR spectra during the first pulse of methanol vapours on the three investigated samples. The spectrum of pure methanol is reported on top for comparison.

Fig. 7: *In situ* ATR-IR spectra in the C–O stretching region recorded over hydrated RM-Pt/TiO_2 under flowing N_2 saturated with methanol vapours at 30°C. The arrows indicate the behavior of the

peak intensities. Inset: temporal dependence of the signals at (□) 1641 cm^{-1}, (●) 1586 cm^{-1} and (▲) 1033 cm^{-1} (scaled by a factor 10).

Fig. 8: ATR-IR spectra recorded at 30°C under flowing N_2 for 10 min on TiO_2 and RM-Pt/TiO_2 after consecutive exposure to (a) methanol vapours, (b) water vapours, and (c) again methanol vapours.

Fig. 9: Effect of increasing methanol-to-water molar fraction *x* on the *in situ* ATR-IR spectra recorded with TiO_2 and RM-Pt/TiO_2 after N_2 purging. The labelled bands are assigned to Pt-CO (2020 cm^{-1}), formaldehyde (1727 cm^{-1}), formic acid (1640 cm^{-1}), formate (1586 and 1360 cm^{-1}) and dimethyl ether (1548 cm^{-1}).

Fig. 10: (a) Effect of UV-vis irradiation under flowing N_2 on the ATR-IR spectra of TiO_2 and RM-Pt/TiO_2 pre-saturated in methanol in the dark (blue curves before UV-vis irradiation and red curves after 2 h irradiation). (b) Teime dependence of the IR baseline due to the formation of photopromoted CB and ST electrons in TiO_2 and RM-Pt/TiO_2. The baseline is represented by the signal at 1900 cm^{-1}.

Fig. 11: Effect of UV-vis irradiation on the ATR-IR spectra of RM-Pt/TiO_2 after methanol saturation and on the reactivity of the surface species after 2 h irradiation in N_2 flow. The blue curves were recorded after methanol saturation in the dark (upper panel), followed by UV-vis irradiation under in flowing N_2 (lower panel). The red curves were recorded with the same sample under constant UV-vis irradiation also during saturation with methanol.

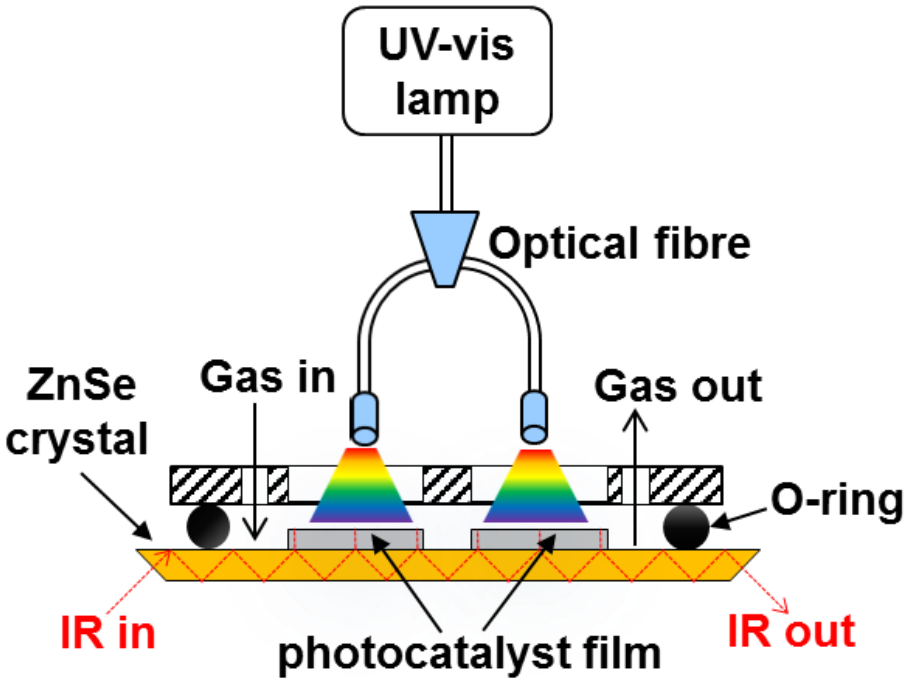

Figure 1

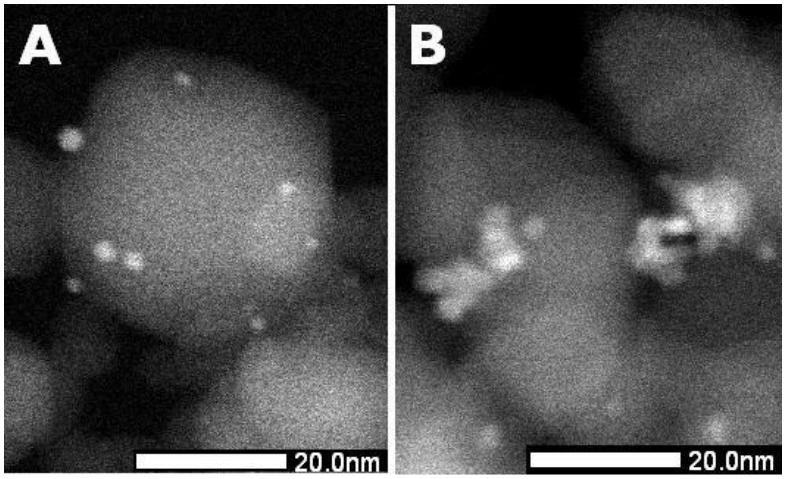

Figure 2

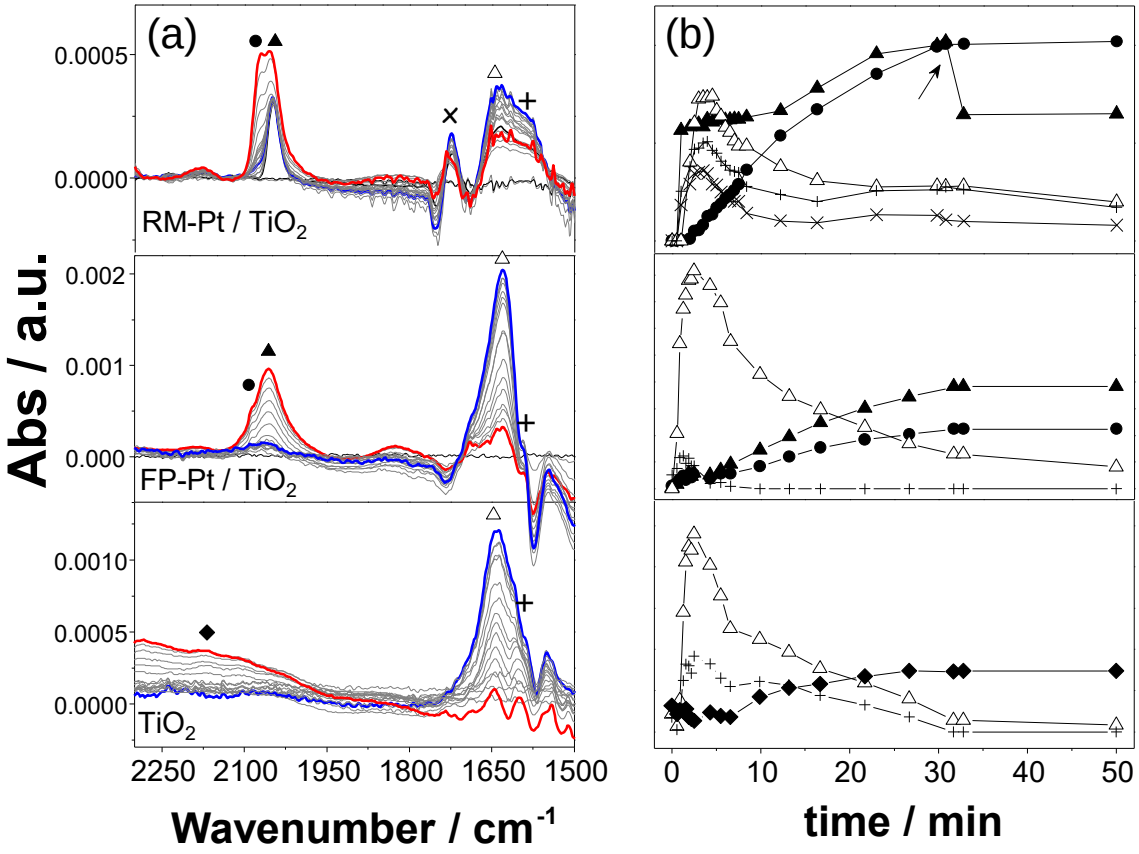

Figure 3

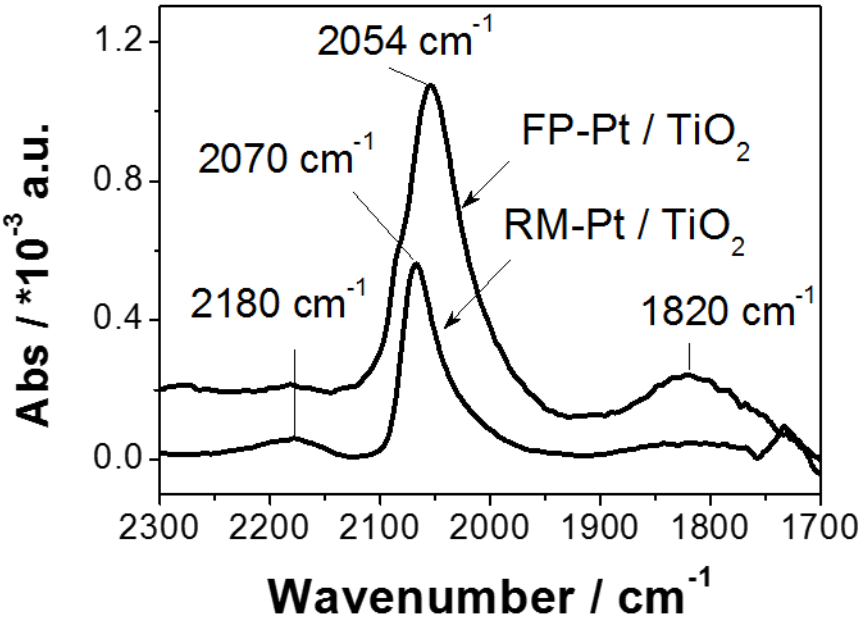

Figure 4

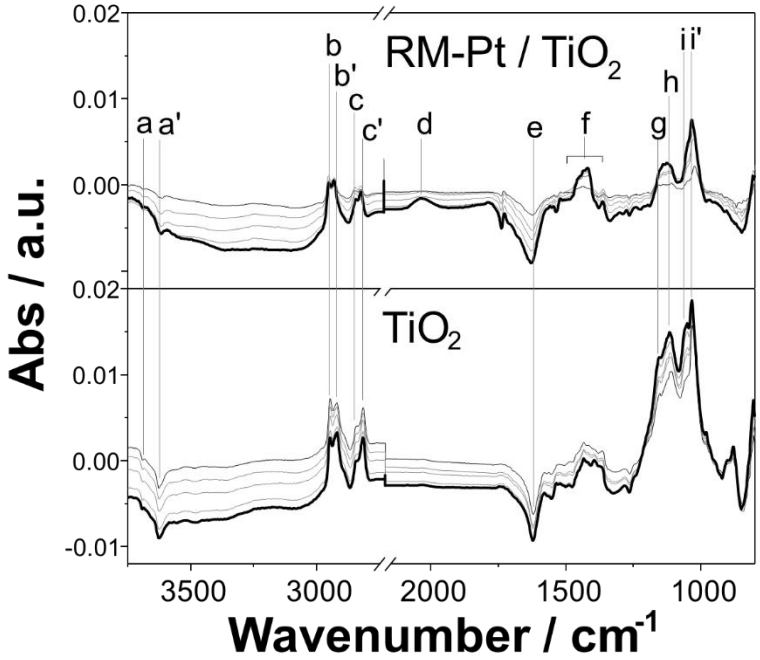

Figure 5

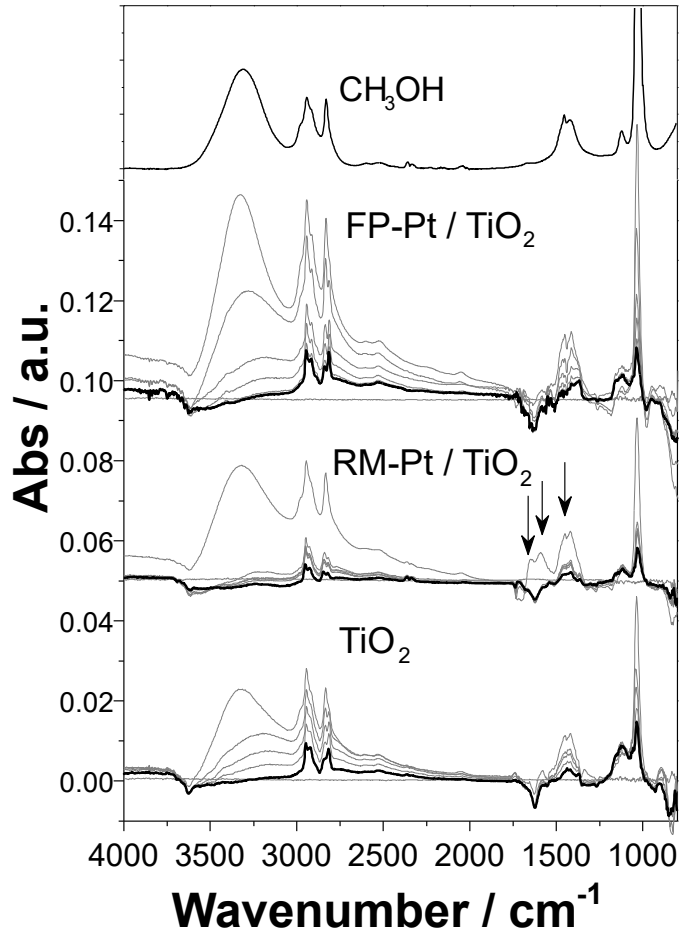

Figure 6

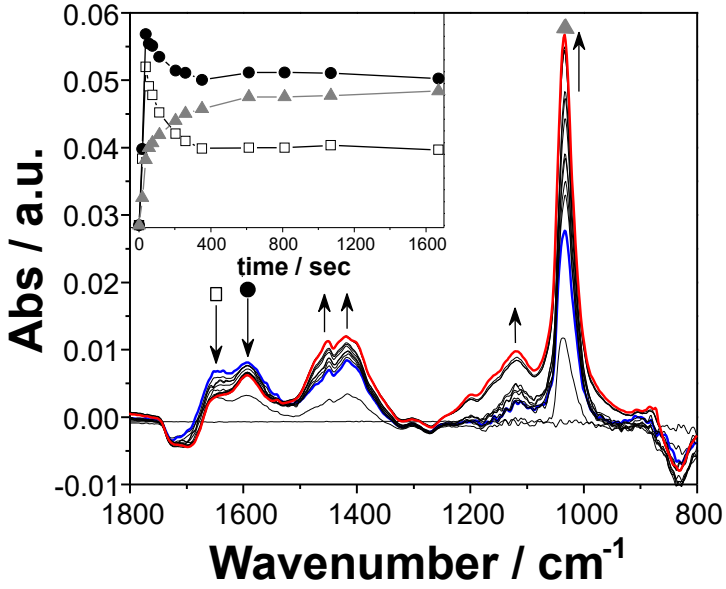

Figure 7

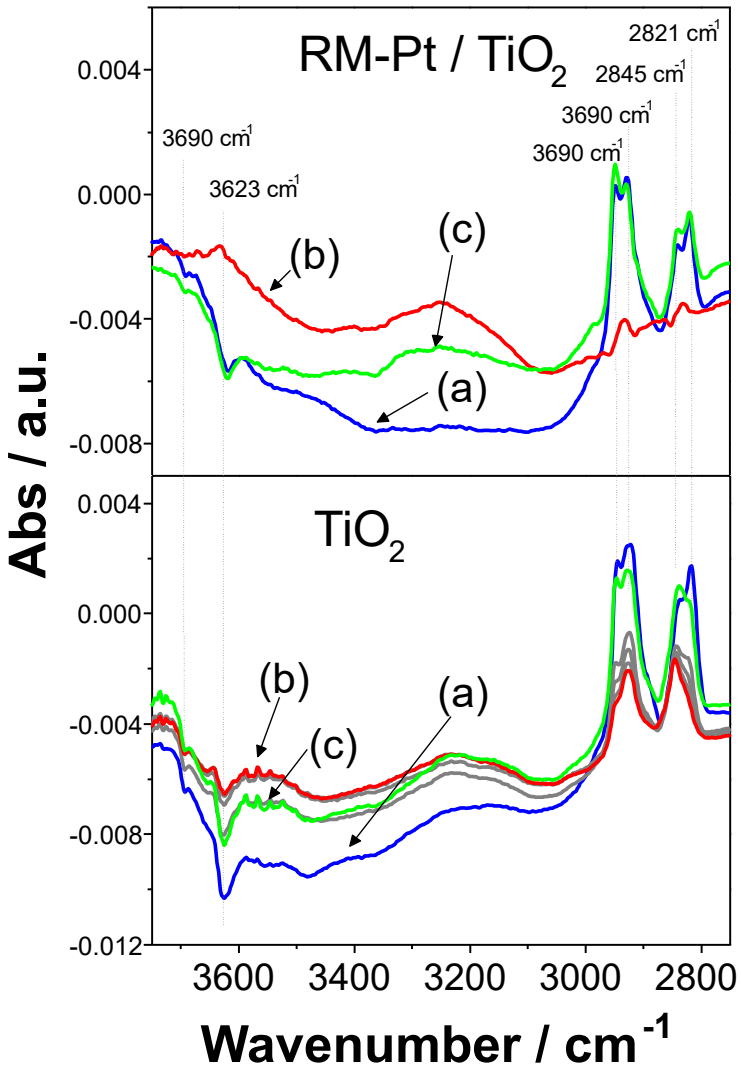

Figure 8

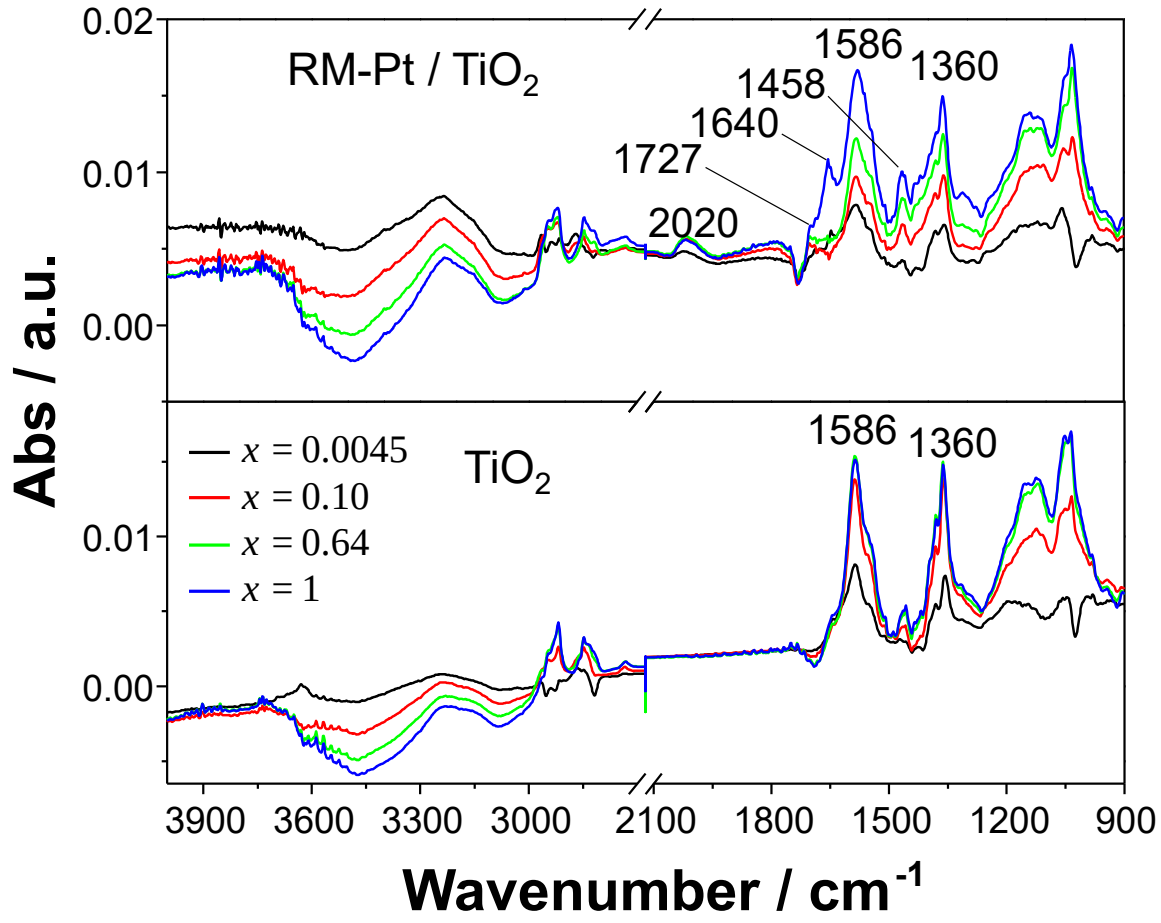

Figure 9

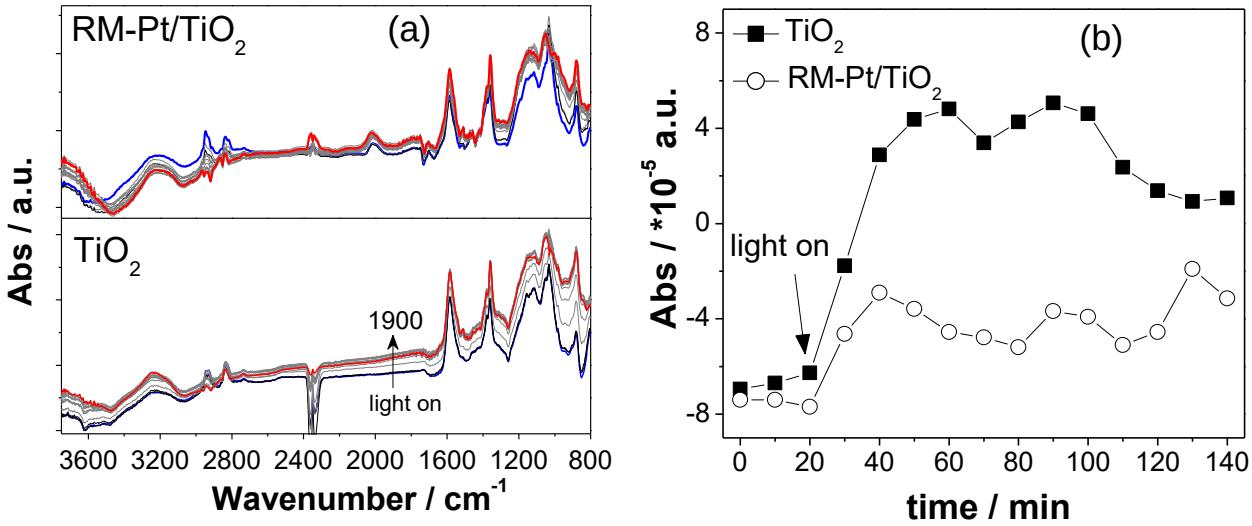

Figure 10

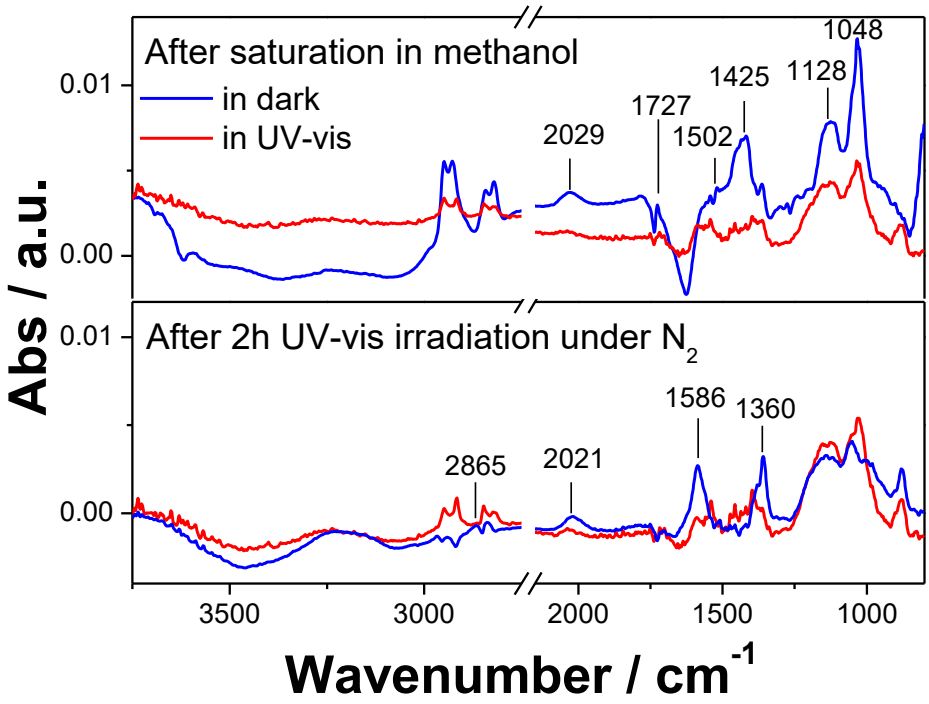
After saturation in methanol
in dark
in UV-vis
2029
1727
1502
1425
1128
1048
After 2h UV-vis irradiation under N2
2865
2021
1586
1360
0.01
0.00
0.01
0.00
Abs / a.u.
3500
3000
2000
1500
1000
Wavenumber / cm-1

Figure 11

References

[1] G.L. Chiarello, M.H. Aguirre, E. Selli, Hydrogen production by photocatalytic steam reforming of methanol on noble metal-modified TiO_2, J. Catal. 273 (2010) 182–190. doi:10.1016/j.jcat.2010.05.012.

[2] G.L. Chiarello, D. Ferri, E. Selli, Effect of the CH_3OH/H_2O ratio on the mechanism of the gas-phase photocatalytic reforming of methanol on noble metal-modified TiO_2, J. Catal. 280 (2011) 168–177. doi:10.1016/j.jcat.2011.03.013.

[3] G.L. Chiarello, A. Di Paola, L. Palmisano, E. Selli, Effect of titanium dioxide crystalline structure on the photocatalytic production of hydrogen, Photochem. Photobiol. Sci. 10 (2011) 355–360. doi:10.1039/C0PP00154F.

[4] M.V. Dozzi, G.L. Chiarello, M. Pedroni, S. Livraghi, E. Giamello, E. Selli, High photocatalytic hydrogen production on Cu(II) pre-grafted Pt/TiO_2, Appl. Catal. B Environ. 209 (2017) 417–428. doi:10.1016/j.apcatb.2017.03.007.

[5] G.L. Chiarello, M.V. Dozzi, M. Scavini, J.-D. Grunwaldt, E. Selli, One step flame-made fluorinated Pt/TiO_2 photocatalysts for hydrogen production, Appl. Catal. B Environ. 160–161 (2014) 144–151. doi:10.1016/j.apcatb.2014.05.006.

[6] E.A. Taylor, G.L. Griffin, Product Selectivity during CH_3OH Decomposition on TiO_2 Powders, (1988) 477–481.

[7] W.-C. Wu, C.-C. Chuang, J.-L. Lin, Bonding Geometry and Reactivity of Methoxy and Ethoxy Groups Adsorbed on Powdered TiO_2, J. Phys. Chem. B. 104 (2000) 8719–8724. doi:10.1021/jp0017184.

[8] A. Yamakata, T.A. Ishibashi, H. Onishi, Electron- and hole-capture reactions on Pt/TiO_2 photocatalyst exposed to methanol vapor studied with time-resolved infrared absorption spectroscopy, J. Phys. Chem. B. 106 (2002) 9122–9125. doi:10.1021/jp025993x.

[9] C. Wang, H. Groenzin, M.J. Shultz, Surface Characterization of Nanoscale TiO_2 Film by Sum Frequency Generation Using Methanol as a Molecular Probe, J. Phys. Chem. B. 108 (2004) 265–272. doi:10.1021/jp0356463.

[10] T. Chen, Z. Feng, G. Wu, J. Shi, G. Ma, P. Ying, et al., Mechanistic studies of photocatalytic reaction of methanol for hydrogen production on Pt/TiO_2 by in situ fourier transform IR and time-resolved IR spectroscopy, J. Phys. Chem. C. 111 (2007) 8005–8014. doi:10.1021/jp071022b.

[11] P. Pichat, Representative examples of infrared spectroscopy uses in semiconductor photocatalysis, Catal. Today. 224 (2014) 251–257. doi:10.1016/j.cattod.2013.11.036.

[12] L. Mino, IR spectroscopy as a tool to investigate photocatalytic reactions at oxide surfaces, Rend. Lincei. 28 (2017) 143–149. doi:10.1007/s12210-016-0592-9.

[13] H. Belhadj, S. Melchers, P.K.J. Robertson, D.W. Bahnemann, Pathways of the photocatalytic reaction of acetate in H_2O and D_2O: A combined EPR and ATR-FTIR study, J. Catal. 344 (2016) 831–840. doi:10.1016/j.jcat.2016.08.006.

[14] D. Gong, V.P. Subramaniam, J.G. Highfield, Y. Tang, Y. Lai, Z. Chen, In Situ Mechanistic Investigation at the Liquid/Solid Interface by Attenuated Total Reflectance FTIR: Ethanol Photo-Oxidation over Pristine and Platinized TiO_2 (P25), ACS Catal. 1 (2011) 864–871. doi:10.1021/cs200063q.

[15] M. El-Roz, P. Bazin, M. Daturi, F. Thibault-Starzyk, Operando Infrared (IR) Coupled to Steady-State Isotopic Transient Kinetic Analysis (SSITKA) for Photocatalysis: Reactivity and Mechanistic Studies, ACS Catal. 3 (2013) 2790–2798. doi:10.1021/cs4006088.

[16] A. Litke, E.J.M. Hensen, J.P. Hofmann, Role of Dissociatively Adsorbed Water on the Formation of Shallow Trapped Electrons in TiO_2 Photocatalysts, J. Phys. Chem. C. 121 (2017) 10153–10162. doi:10.1021/acs.jpcc.7b01151.

[17] J. Liu, L. Zhang, X. Yao, S.S.C. Chuang, Photo-generated conduction-band and shallow-trap electrons from UV irradiation on ethanol-adsorbed TiO_2 and N-TiO_2: an in situ infrared

study, Res. Chem. Intermed. 43 (2017) 5041–5054. doi:10.1007/s11164-017-3038-9.
[18] A. Yamakata, T. Ishibashi, H. Onishi, Effects of water addition on the methanol oxidation on Pt/TiO_2 photocatalyst studied by time-resolved infrared absorption spectroscopy, J. Phys. Chem. B. 107 (2003) 9820–9823. doi:10.1021/jp034997e.
[19] Y. Attia, M. Samer, Metal clusters: New era of hydrogen production, Renew. Sustain. Energy Rev. 79 (2017) 878–892. doi:10.1016/j.rser.2017.05.113.
[20] G.L. Chiarello, I. Rossetti, L. Forni, Flame-spray pyrolysis preparation of perovskites for methane catalytic combustion, J. Catal. 236 (2005) 251–261. doi:10.1016/j.jcat.2005.10.003.
[21] C.-C. Chuang, W.-C. Wu, M.-C. Huang, I.-C. Huang, J.-L. Lin, FTIR Study of Adsorption and Reactions of Methyl Formate on Powdered TiO_2, J. Catal. 185 (1999) 423–434. doi:http://dx.doi.org/10.1006/jcat.1999.2516.
[22] F. Boccuzzi, A. Chiorino, M. Manzoli, FTIR study of methanol decomposition on gold catalyst for fuel cells, J. Power Sources. 118 (2003) 304–310. doi:10.1016/S0378-7753(03)00075-2.
[23] F.P. Rotzinger, J.M. Kesselman-Truttmann, S.J. Hug, V. Shklover, M. Grätzel, Structure and Vibrational Spectrum of Formate and Acetate Adsorbed from Aqueous Solution onto the TiO_2 Rutile (110) Surface, J. Phys. Chem. B. 108 (2004) 5004–5017. doi:10.1021/jp0360974.
[24] A. Lukaski, Photocatalytic oxidation of methyl formate on TiO_2: a transient DRIFTS study, J. Catal. 223 (2004) 250–261. doi:10.1016/j.jcat.2003.12.015.
[25] M.D. Hernández-Alonso, I. Tejedor-Tejedor, J.M. Coronado, M.A. Anderson, J. Soria, Operando FTIR study of the photocatalytic oxidation of acetone in air over TiO_2–ZrO_2 thin films, Catal. Today. 143 (2009) 364–373. doi:10.1016/j.cattod.2009.02.033.
[26] J.G. Highfield, M.H. Chen, P.T. Nguyen, Z. Chen, Mechanistic investigations of photo-driven processes over TiO_2 by in-situ DRIFTS-MS: Part 1. Platinization and methanol reforming, Energy Environ. Sci. 2 (2009) 991. doi:10.1039/b907781m.
[27] F. Boccuzzi, A. Chiorino, M. Manzoli, FTIR study of the electronic effects of CO adsorbed on gold nanoparticles supported on titania, Surf. Sci. 454 (2000) 942–946. doi:10.1016/S0039-6028(00)00160-6.
[28] F.M. Leibsle, R.S. Sorbello, R.G. Greenler, Coupled harmonic oscillator models of carbon monoxide adsorbed on stepped, platinum surfaces, Surf. Sci. 179 (1987) 101–118. doi:10.1016/0039-6028(87)90122-1.
[29] R.K. Brandt, M.R. Hughes, L.P. Bourget, K. Truszkowska, R.G. Greenler, The interpretation of CO adsorbed on Pt/SiO_2 of two different particle-size distributions, Surf. Sci. 286 (1993) 15–25. doi:10.1016/0039-6028(93)90552-U.
[30] H. Gao, W. Xu, H. He, X. Shi, X. Zhang, K. ichi Tanaka, DRIFTS investigation and DFT calculation of the adsorption of CO on Pt/TiO2, Pt/CeO_2 and $FeOx/Pt/CeO_2$, Spectrochim. Acta - Part A Mol. Biomol. Spectrosc. 71 (2008) 1193–1198. doi:10.1016/j.saa.2008.03.036.
[31] B. Ni, X. Wang, Face the Edges: Catalytic Active Sites of Nanomaterials, Adv. Sci. 2 (2015) 1500085. doi:10.1002/advs.201500085.
[32] S. Bates, M. Gillan, G. Kresse, Adsorption of methanol on TiO_2 (110): A first-principles investigation, J. Phys. Chem. 2 (1998) 2017–2026. doi:10.1021/jp9804998.
[33] A. Tilocca, A. Selloni, Methanol Adsorption and Reactivity on Clean and Hydroxylated Anatase(101) Surfaces, J. Phys. Chem. B. 108 (2004) 19314–19319. doi:10.1021/jp046440k.
[34] Y. Han, C. Liu, Q. Ge, Effect of Pt Clusters on Methanol Adsorption and Dissociation over Perfect and Defective Anatase TiO_2 (101) Surface, J. Phys. Chem. C. 113 (2009) 20674–20682. doi:10.1021/jp907399j.
[35] A. Nuhu, J. Soares, M. Gonzalez-Herrera, A. Watts, G. Hussein, M. Bowker, Methanol oxidation on Au/TiO_2 catalysts, Top. Catal. 44 (2007) 293–297. doi:10.1007/s11244-007-0302-z.
[36] G. Busca, H. Saussey, O. Saur, J.C. Lavalley, V. Lorenzelli, FT-IR characterization of the

surface acidity of different titanium dioxide anatase preparations, Appl. Catal. 14 (1985) 245–260. doi:10.1016/S0166-9834(00)84358-4.
[37] F. Guzman, S.S.C. Chuang, Tracing the reaction steps involving oxygen and IR observable species in ethanol photocatalytic oxidation on TiO_2, J. Am. Chem. Soc. 132 (2010) 1502–1503. doi:10.1021/ja907256x.
[38] Z. Yu, S.S.C. Chuang, In situ IR study of adsorbed species and photogenerated electrons during photocatalytic oxidation of ethanol on TiO_2, J. Catal. 246 (2007) 118–126. doi:10.1016/j.jcat.2006.11.022.
[39] G.A. Flores-Escamilla, J.C. Fierro-Gonzalez, Infrared spectroscopic study of dimethyl ether carbonylation catalysed by TiO_2 -supported rhodium carbonyls, Catal. Sci. Technol. 5 (2015) 843–850. doi:10.1039/C4CY00912F.
[40] L. Zhang, R. Dillert, D. Bahnemann, M. Vormoor, Photo-induced hydrophilicity and self-cleaning: models and reality, Energy Environ. Sci. 5 (2012) 7491–7507. doi:10.1039/c2ee03390a.